ROYAL SOCIETY
OF CHEMISTRY

Check for updates

Amino-alcohol functionalized porous polymer coupled with chromium hydroxide nanoparticles for efficient Cd(II) adsorption from aqueous solutions†

Hamida Y. Mostafa,[a] Ahmed M. Masoud, [b] Adel A. El-Zahhar, [c]
Majed M. Alghamdi,[c] Entsar H. Taha,[d] Ahmed M. A. El Naggar [*a]
and Mohamed H. Taha [b]

Cadmium is one of the most hazardous heavy metal contaminants, and it is usually abundant in the wastewater released from paint and pigment industries. Such effluents urgently need to be treated before their proper reuse for various industrial and agricultural purposes. Therefore, in this study, the process of Cd(II) ion adsorption from waste aqueous-solutions was investigated using polystyrene (PS), ethanolamine-modified polystyrene (EA-PS), and chromium hydroxide-impregnated ethanolamine-modified polystyrene (Cr@EA-PS) as new effective sorbents. The structural and textual properties as well as the surface charges and particle sizes of the prepared sorbents were examined using Fourier transform infrared (FTIR) spectroscopy, scanning electron microscopy (SEM), N_2 adsorption–desorption surface area analysis, X-ray diffraction (XRD), dynamic light scattering (DLS) and zeta potential analysis. Herein, correlations between different features of the three adsorbents and their impacts on adsorption efficiency were extensively investigated. Adsorption kinetics and isotherm studies were also conducted to evaluate the sorption mechanisms and the achieved capacities of the presented adsorbents. Results showed that surface functionalization with ethanol amine particles significantly improved adsorption capacity owing to the introduction of amino groups, providing further interactions with heavy metal species. Moreover, the subsequent impregnation of $Cr(OH)_3$ into the EA-PS structure could successively enhance surface properties and porosity, leading to observation of the highest adsorption capacity (13.6 mg g^{-1} for Cr@EA-PS). Such increased adsorption capacity is nearly 10-fold higher than the reported capacity of PS. Kinetic studies revealed that the adsorption process followed a pseudo-second-order model, indicating chemisorption as the primary adsorption mechanism. Isotherm analysis confirmed a favorable monolayer adsorption process exhibited by the three structures. The combination of chemical bonding and physical adsorption mechanisms was observed for Cr@EA-PS, explaining its performance superiority in removing Cd(II) ions. Thus, the inorganic–organic composite exhibits the highest potential among the three introduced sorbents for practical applications in the field of wastewater treatment.

1. Introduction

Owing to the lack of clean freshwater sources, the world is currently experiencing a shortage of clean drinking water. This problem is exacerbated by environmental pollutants entering the food chain through agriculture irrigation and drinking water.[1] Elements with atomic weights between 63.5 and 200.6 as well as specific gravities higher than 5.0 are classified as heavy metals.[2] Heavy metal-contaminated wastewater is released into the environment either directly or indirectly as a result of rapid industrial development, particularly in emerging nations. Heavy metals are nonbiodegradable, unlike organic pollutants, and they tend to accumulate in living organisms. Many heavy metal ions are also known to be hazardous or carcinogenic. Among those heavy metals, cadmium is of particular concern as it is one of the highly toxic species present in industrial wastewater.[3–5]

[a]*Egyptian Petroleum Research Institute (EPRI), Nasr City, 11727, Cairo, Egypt. E-mail: drmeto1979@yahoo.com*

[b]*Nuclear Materials Authority, P. O. Box 530, El Maadi, Cairo, Egypt*

[c]*Department of Chemistry, Faculty of Science, King Khalid University, Abha 9004, Saudi Arabia*

[d]*Department of Plant Protection, Faculty of Agriculture, Ain Shams University, Egypt*

The presence of cadmium ions in wastewater poses potential ecological concerns. It degrades slowly and can be found in wastewater in a number of different forms. Furthermore, it is acknowledged to have no biological purpose and mainly pollutes aquatic life. The primary sources of Cd(II)-contaminated wastewater include industrial discharges from mining operations, alkaline batteries, pigments, fertilizers, pesticides, ceramics, combustion of specific oils, mining activities, and electroplating/metal plating. The maximum permitted level of cadmium in drinking water is 5 μg L^{-1}.[6–8] Contaminated water is the main source through which millions of humans have absorbed increased doses of heavy metals, especially in developing countries.[9,10] Studies have indicated that the accumulation of Cd in living organisms might result in various detrimental effects. For instance, it has been found that Cd promotes organ failure and cancer in humans.[11,12] As a result, proper disposal of these components is desperately needed. Numerous approaches, including ion-exchange, electrochemical procedures, membrane filtration, chemical precipitation, and reverse osmosis, have been used in previous investigations.[13] However, significant financial and technical obstacles may still stand as a major restriction for the wide use of these methods to remove huge quantities of Cd from wastewater.[14]

Adsorption technologies have been popular in the treatment of large contaminated water bodies due to their cost-effective materials, and the advantage of being an environmentally acceptable method in treating heavy metal pollution.[15,16] High-efficiency and the use of inexpensive adsorptive materials are key essential points to successfully achieve efficient adsorption processes. High affinity toward the targeted pollutants is a necessary point in assessing the quality of effective sorbents. Ideally, they should be able to quickly and efficiently adsorb multiple contaminants at once. As such, polymers and polymer-composite materials are appealing substitutes for traditional adsorbents.[17–19]

Vinyl polymer (in general) and polystyrene (particularly) are both considered thermoplastic resins. PS is a lengthy hydrocarbon chain that is composed of connected vinyl groups, where each one is bonded with a phenyl group. Free radical polymerization is one of the techniques used for preparing PS, in which styrene monomers (phenyl-ethene) are attacked by polymerization initiator radicals.[20] The major characteristics of polystyrene rely heavily on the presence of pendant phenyl (C$_6$H$_5$) groups. Specifically, these ring-shaped chemical groups keep the polymer chains from packing tightly into crystalline configurations, making solid polystyrene a transparent material. The phenyl rings also prevent the chains from rotating around the carbon–carbon bonds, contributing to the polymer's well-known stiffness. Additionally, these rings can conserve the ordered arrangements of the PS unit, leading to a highly open structure for efficient adsorption applicability.[21] A variety of applications for synthetic polymers, such as polystyrene and its derivatives, have been discovered over the past decades. The surface modifications of polymers (generally) and PS (specifically) can improve their surface area values, and increase the availability of surface functional groups. Consequently, such structures can be effectively employed in the adsorption processes of metals from different specimens, owing to their enhanced capabilities to adsorb such cationic species. Thus, the removal of harmful metals, especially toxic and carcinogenic ones, from our environment can be successfully achieved.[22]

This research work introduces novel adsorbents based on a combination of polystyrene (PS) with ethanolamine, followed by impregnation of chromium hydroxide nanoparticles (Cr@EA-PS) for efficient removal of cadmium (Cd(II)) ions from aqueous solutions. The study focuses on evaluating the adsorption performance of the developed materials under various pH conditions, contact time, sorbent dosage, and initial Cd(II) concentration. The novelty of this work is based on the dual modification of polystyrene to enhance its adsorption capacity through the introduction of amino groups (from ethanolamine), followed by impregnating chromium hydroxide nanoparticles using ultrasonic homogenization. Such modification effectively enhances the surface features of the obtained composite and expands its functional group content, in comparison to blank PS. The structural, morphological, surface characteristics, and surface charges of the presented adsorbents were comprehensively analyzed using several analytical techniques. Kinetic and isotherm studies were conducted to elucidate the adsorption exploits and mechanisms by the introduced structures. The cost-effectiveness and suitability of Cr@EA-PS as a proper adsorbent for remediation of heavy metal-contaminated wastewater are highlighted at the end of this investigation.

2. Experimental

2.1. Materials

Styrene, potassium persulfate, and sodium dodecyl sulfate were purchased from Sigma-Aldrich Co (St Louis, MO, USA). The reagents were used as received with no further treatments. Cadmium sulfate (CdSO$_4$) was provided by Sigma-Aldrich (St. Louis, MO, USA), and used to prepare 1.0 g L^{-1} of metal stock solutions using double-distilled water. Before the sorption tests, the solutions were freshly made for the studies by dilution with double-distilled water to the appropriate concentration. For the desorption tests, sulfuric, hydrochloric, and nitric acids were provided by Merck KGaA (Darmstadt, Germany), and all acids were of analytical grade.

2.2. Synthesis of the sorbents

Polystyrene was synthesized *via* high internal phase emulsion polymerization technique. Experimentally, styrene (4.96 g) was mixed with sodium dodecyl sulfate (0.494 g) as a surfactant, producing the oil phase for PS synthesis. The mixture was then added to 11 mL of deionized water at 60 °C under stirring, forming an emulsion. Potassium persulfate (0.23 g) was then added to the mixture as an initiator to start the polymerization. The mixture was kept under stirring for 2 h at 60 °C. Subsequently, the emulsion was dried in an oven at 60 °C for 12 h to obtain the PS polymer.[23] PS was then blended with ethanolamine through impregnating a certain weight (3 g) of polymer

Table 1 The main variables and fixed parameters of the Cd(II) adsorption experiments

Adsorption parameters	Variables	Fixed conditions
Solution pH	2–9	Sorbent dose 3.0 g L^{-1}, initial concentration of 50 mg L^{-1}, time 120 min, room temperature
Time, min	5–600	Solution pH of 6.01, sorbent dose 3.0 g L^{-1}, initial concentration of 50 mg L^{-1}, room temperature
Sorbent dose, g L^{-1}	1–5	Initial concentration of 50 mg L^{-1}, time 120 min, Solution pH of 6.01, room temperature
Initial concentration, mg L^{-1}	3–300	Solution pH of 6.02, time 120 min, sorbent dose 3.0 g L^{-1}, room temperature

in 10 mL of EA under vigorous stirring and heating at 50 °C for 15 min. Then, the final obtained organic composite (EA-PS) was filtered and dried for 6 h. Separately, nanoparticles of Cr(OH)$_3$ were prepared *via* chemical precipitation method, as reported in ref. 23. Practically, 0.2 M solution of chromium salt was prepared *via* dissolving anhydrous chromium nitrate (Cr(NO$_3$)$_3$) in double-distilled water under vigorous stirring (500 rpm) using a magnetic stirrer, which was set at 80 °C. Upon observing the formation of a clear solution, the dropwise addition of ammonia solution (35 wt%) proceeded until a pH value of 10 was achieved. Subsequently, the obtained Cr(OH)$_3$ species were left to settle down at the bottom of the reaction vessel for 45 min. The particles of the metal hydroxide were then collected *via* centrifugation at 5000 rpm, washed several times by double-distilled water, and dried at 70 °C inside a vacuum oven for 2 h. Consequently, particles of Cr(OH)$_3$ were impregnated with the organic composite under the effect of ultrasonic waves. Specifically, 0.2 g of metal hydroxide was mixed with 0.8 g of EA-PS structure in 25 mL of ethanol, where the whole mixture was exposed to ultrasonication (60 W) for 20 min. Then, the final produced composite (denoted as Cr@EA-PS) was collected *via* filtration and vacuum-dried at 60 °C to ensure the complete release of ethanol molecules.

2.3. Sorbent characterization

Several analytical tools were used to determine the essential characteristics (such as structural, morphological, and surface features) of the prepared structures. X-ray diffraction (XRD) patterns were collected *via* Cu Kα X-ray radiation operated at λ = 1.540 Å (PAN analytical X'PERT Pro, Germany). Fourier transform infrared (FTIR) spectroscopy was used to detect the functional groups of the prepared samples in the range of 4000–400 cm^{-1} *via* the KBr pellet method using a PerkinElmer spectrometer (Spectrum One, USA). A scanning electron microscope (SEM), JEOL-JSM (model no: 6360) equipped with EDX was employed to confirm the morphological structure of the introduced adsorbents in this study. The surface characteristics of these structures were recorded by an ANOVA 3200, USA apparatus using the adsorption–desorption isotherms of nitrogen at −196 °C. Zeta potential and particle size distribution of the examined materials were obtained *via* the Zetasizer device model 3180, Malvern, UK.

2.4. Sorption tests

In the current investigation, the efficiency of polystyrene and the functionalized polystyrene sorbents toward Cd(II) removal ions from aqueous solution was explored. The practical studies

were carried out in polypropylene tubes containing a pre-determined volume of the aqueous phase (*V*, L) and a defined weight of the sorbent material (*m*, g). The components were mixed in a SWB 27–27 L thermo-shaker water bath for pre-determined time intervals (*t*, min). Cadmium(II) was initially added at a concentration of (C_0; 50 mg L^{-1}), and the pH of the mixture was kept constant using 0.5 M HCl and 0.5 M NaOH. The pH values were measured with a Cyber Scan pH 6000 pH-meter (Eutech Instruments, Netherlands). A 1.2 μm filter membrane was used to filter the mixture after the completion of the designated shaking times during this study. Regarding the investigation plan, the main studied variables and fixed parameters are summarized in Table 1. A desorption investigation was conducted using an analogous experimental protocol. Specifically, a fixed volume of eluent (nitric acid, hydrochloric acid, or sulfuric acid) was combined with the spent sorbents (applying a dose of 3.0 g L^{-1}) for 4 h, followed by filtration. The concentration of Cd(II) in the collected filtrate was then measured to determine the desorption efficiency and the released amount of the adsorbed metal ions. Five consecutive cycles of adsorption and desorption were examined to understand the performance consistency and sustainability of the sorbent.

In all conducted experiments, an atomic absorption spectrometer GBC 932 AA (UK) was used to assess the initial concentration (C_0, mg L^{-1}) and the final residual concentration (C_e, mg L^{-1}) of Cd(II). The samples were filtered using 0.22 mm filters before they were subjected to analysis. Only a relative error mean value of ≤5% was deemed acceptable after executing each experimental run in triplicate. Eqn (1)–(3) were used to calculate the sorption efficiency (*E*%), sorption capacity (q_e, mg g^{-1}), and distribution coefficient (K_d):

$$q_e = (C_0 - C_e) \times \frac{V}{m} \tag{1}$$

$$R\% = \frac{(C_0 - C_e)}{C_0} \times 100 \tag{2}$$

$$K_d = \frac{q_e}{C_e} \tag{3}$$

3. Results & discussion

3.1. Sorbent characterization

The structural characteristics of the three presented structures in this research study are discussed through the provided FTIR and XRD spectra in Fig. 1 and 2, respectively. For the as-prepared polystyrene polymer, the structural features are
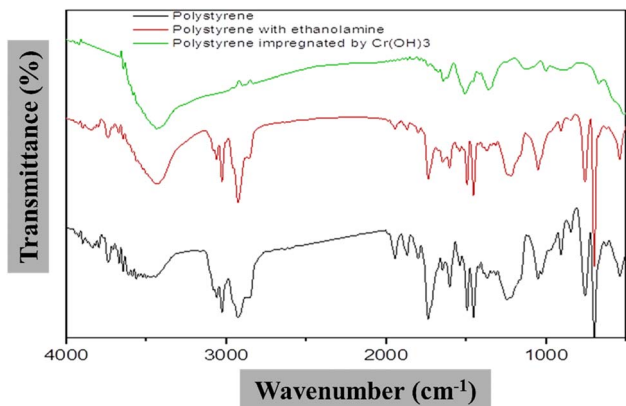
Fig. 1 FTIR of polystyrene, ethanolamine-blended polystyrene, and Cr(OH)$_3$-impregnated polystyrene/ethanolamine.

illustrated through the provided FTIR spectrum in Fig. 1. The observed peaks around 3025 and 2920 cm^{-1} correspond to both aromatic and aliphatic C–H stretching vibrations, respectively.[23] Additionally, the presented peaks at 1601 and 1492 cm^{-1} are attributed to the C=C stretching vibrations of the benzene ring.[24] The peaks around 760 and 698 cm^{-1} belong to the C–H out-of-plane bending vibrations of the mono-substituted benzene rings.[23] The observed characteristic peaks are consistent with the literature reports for polystyrene.[25,26] For the ethanolamine-modified polystyrene structure, some additional absorption bands alongside those belonging to the polystyrene were observed. Particularly, a broad peak at around 3300 cm^{-1}

that is assigned to the N–H stretching vibration of the amine group was detected.[27] The peaks around 2920 and 2850 cm^{-1} are likely due to the aliphatic C–H stretching vibrations of the ethanolamine moiety.[28] The peak at 1640 cm^{-1} can be attributed to the N–H bending vibration of the amine group.[27,28] These results are in agreement with previous studies on amine-functionalized polymers, as reported in ref. 27 and 28. Conversely, the spectrum of the ethanolamine-combined polystyrene impregnated by Cr(OH)$_3$ displays an additional peak at around 3400 cm^{-1}, which can be assigned to the O–H stretching vibration of the Cr(OH)$_3$ species.[29] The observed peak around 1375 cm^{-1} is related to the Cr–O stretching vibration in Cr(OH)$_3$.[30] Overall, the provided FTIR spectra confirm the successful synthesis of polystyrene and its subsequent composites with ethanolamine, either individually or coupled with the impregnation of Cr(OH)$_3$ using ultrasound waves. The spectra show the characteristic peaks of each component, indicating the presence of the desired functional groups and chemical species that can act as efficient sorbents for the removal of heavy metal particles from the wastewater sample.

In the provided XRD pattern for PS (Fig. 2a), a broad peak centered at $2\theta \approx 21°$ that is characteristic of the present carbon species in polystyrene is observed.[25,26] The broadness of the detected peak reflects the typical amorphous structure of polystyrene, as these polymeric materials lack the long-range ordered crystalline nature. EA-PS (Fig. 2b) showed an XRD pattern that was nearly similar to that of PS. However, the broad peak is slightly shifted and centered at $2\theta \approx 20°$. Additionally,
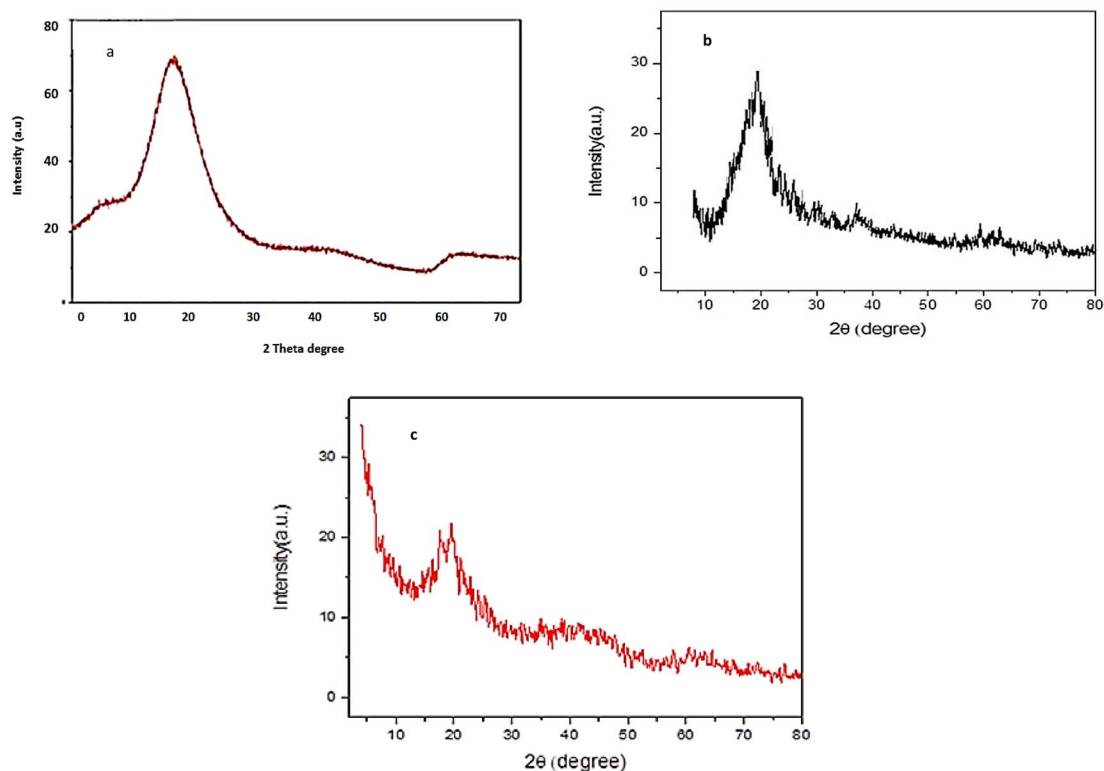

Fig. 2 XRD patterns of (a) PS, (b) EA-PS and (c) the Cr(OH)$_3$-impregnated polystyrene/ethanolamine composite.

the broadness of the observed peak was slightly reduced. The observed shift in the peak position and reduction in its broadness are attributed to the blending of PS with particles of ethanolamine. This leads to some morphological rearrangements due to adhesion between the ethanolamine particles, reducing the amorphous nature of the PS particles. For the Cr@EA-PS composite (Fig. 2c), there is a further shift for the carbon-indicative signal, centering at around 19°, and an obvious decrease in its broadness. Such observations, in addition to the decline of the C peak intensity, refer to the loading of the chromium hydroxide species. Several sharp and intense peaks are present in the XRD pattern, embedded in the broad signal of polystyrene. These peaks can be attributed to the presence of crystalline $Cr(OH)_3$ particles impregnated within the polystyrene matrix.[29] The most prominent sharp XRD signals observed at 2θ values of approximately 15.2, 24.1, 33.7, 35.5, 39.6, 49.5, 54.1, 61.6, and 64.6° are characteristic of hexagonal crystalline $Cr(OH)_3$ (JCPDS card no. 33-0455).[29,30] The relatively high intensities of the $Cr(OH)_3$ peaks suggest that the impregnated metal-hydroxide particles may have a crystallite growth onto the polystyrene structure. Additionally, the observation of such intensities for these XRD signals refers to the presence of an increased number of metal-hydroxide crystals within the investigated composite structure. Therefore, it can be concluded that the impregnation of Cr-hydroxide successfully shifts the structure of the final composite into a mixed amorphous-crystalline nature.[29,30] This shift provides a positive impact by stimulating the adsorption performance of the introduced composite in this study. Specifically, the enhancement of the crystallinity degree is directly correlated with enhancing the sorption capability of the composite in terms of having ordered arrangements of $Cr(OH)_3$ particles. Hence, the additional active sites and improved structure porosity may be involved during the process of capturing Cd(II) ions. Thus, the structural improvements illustrated in the XRD analysis support the presence of an efficient adsorbent with $Cr(OH)_3$ impregnation for heavy metal removal.

The morphologies of the introduced structures are illustrated through the given SEM images in Fig. 3. For blank polystyrene, the displayed SEM image shows a relatively non-uniform and rough surface morphology, which is potentially due to the agglomeration of some polystyrene molecules during the preparation stage.[25–27] Therefore, the detected PS polymer species in the given images are of relatively large sizes, and appear to be in the range of a few micrometers. However, the detected surface roughness probably suggests the enhancement of the adsorption properties by such structure in terms of providing an increased active area and active sites during the removal process. Furthermore, the investigated polymer exhibited a very porous surface, with some observed pores having different diameters.[25,26] After modification with ethanolamine, there is an observable change in the surface, owing to the display of a uniformly smooth morphology. This change can be attributed to the association of some EA particles via hydrogen bonding, forming a monolayer at the surface of the PS particles.[27,28] The noted smooth surface shows a slightly porous

and uneven texture with numerous cavities due to the PS coverage by EA molecules.[27,28]

Upon incorporating $Cr(OH)_3$ into the organic composite using ultrasonication, radical changes in the surface morphology were clearly observed. In particular, the surface appears to be smoother with more uniformity and regular texture compared to the previous structures. Additionally, there are distinct clusters or aggregates of particles visible on the surface, which are likely due to the impregnated $Cr(OH)_3$ species.[29,30] Moreover, the presence of the metal hydroxide species resulted in the observance of a highly porous nature for the hybrid composite in comparison to the other two organic structures. The $Cr(OH)_3$ particles exhibited crystals with different shapes; namely, spherical, tetrahedral, and pentagonal ones.[29,30] Overall, the SEM images clearly show the progressive changes in the surface morphology as the polystyrene particles undergo modification with ethanolamine, and subsequently through impregnation of the $Cr(OH)_3$ species. The introduction of functional groups and the subsequent impregnation process resulted in increased surface smoothness, porosity, and the formation of additional surface features. These morphological changes significantly enhance the adsorption properties of the sorbents presented in this research work.

Further exploration of the particle sizes and surface charges of the illustrated adsorbents are provided through both DLS and zeta potential data, as presented in Fig. 4. An average particle size of 794.8 nm is detected for the polystyrene structure, as presented in Fig. 4a. The size distribution curve indicates that the majority of the particles are in the range of 500–1100 nm, with a significant fraction at around 800 nm. Another low intensity peak located between 150 and 400 nm was observed for this structure, indicating the presence of a few polystyrene molecules in such size range. The observation of a high intensity peak in the distribution curve suggests a relatively uniform particle size for the polystyrene structure.[25,26] For the ethanolamine-modified polystyrene, the average particle size subsequently decreased to 558.5 nm. Additionally, the size distribution curve becomes slightly broader, indicating a wider range of particle sizes, which reveals a shift towards smaller sizes compared to the blank polystyrene. This change in the distribution curve is due to the effect of distributing ethanolamine particles onto the polystyrene surface. Hence, the overall properties of the organic composite are changed because of the potential aggregation behavior due hydrogen bonding between the ethanolamine particles.[27,28] After impregnating the polystyrene-ethanolamine structure by $Cr(OH)_3$, a further decrease in the average particle size (453.1 nm) was observed. The size distribution curve shows a broader range of particle sizes, with an obvious significance for the particles in the range of 400–500 nm. The decline of the average particle sizes is explained by the incorporation of metal hydroxide particles, which are of smaller sizes than the polymer species.[29,30] It is worth noting that the DLS technique measures the hydrodynamic diameter, which includes the sorbent particle and any solvation layers or adsorbed species on the surface. Therefore, the observed changes in the particle size distribution can be
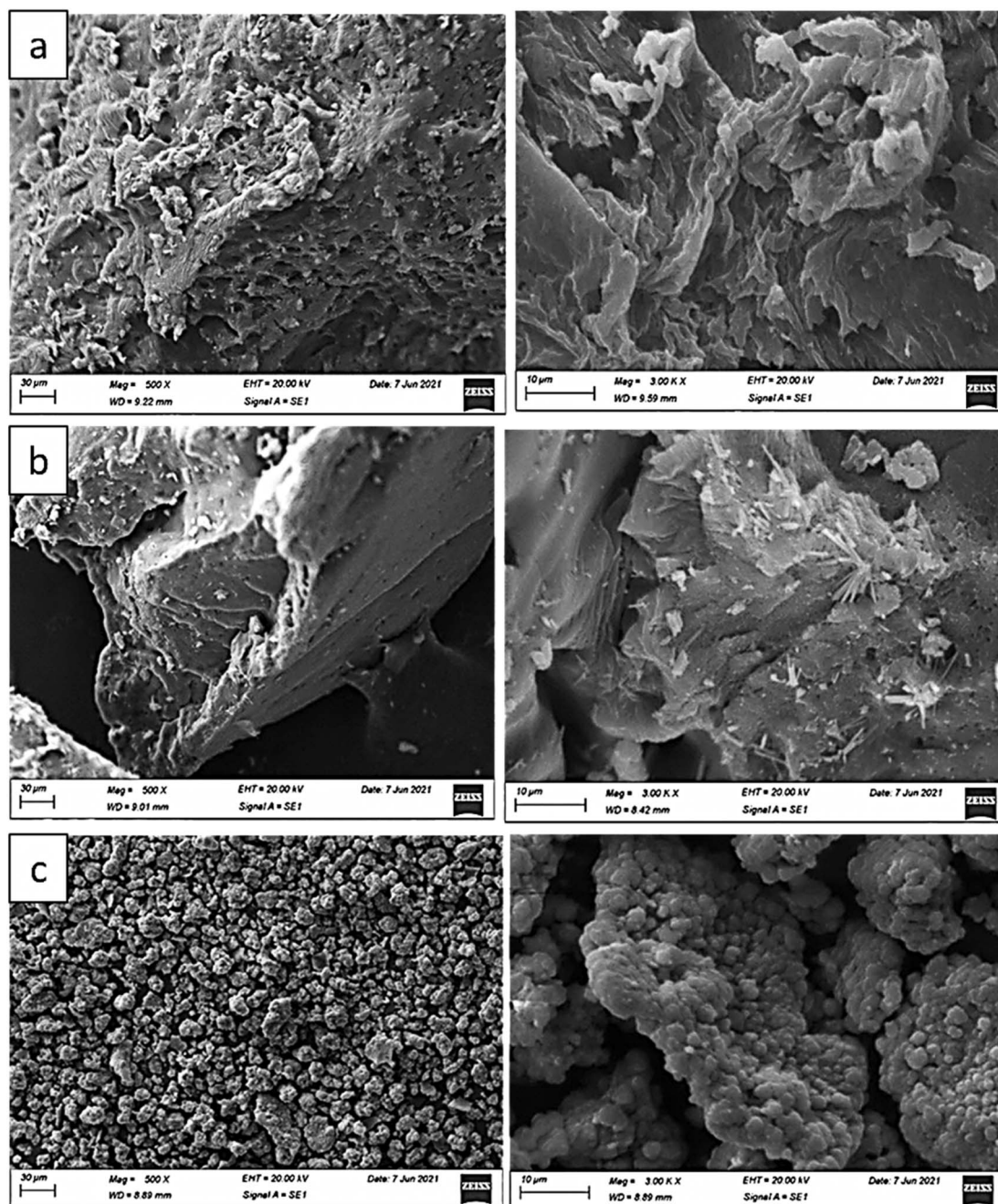
Fig. 3 SEM image of (a) polystyrene, (b) ethanolamine-blended polystyrene, (c) Cr(OH)$_3$-impregnated polystyrene/ethanolamine.

attributed to the modifications made to the PS structure, affecting its surface properties, aggregation behavior, and potential solvation layers.[27–30]

The zeta potential value of the unmodified polystyrene was found to be −17.4 mV, indicating its moderate colloidal stability within a processing system since such value lies between +30 and −30 mV. The observed negative value suggests the presence of some anionic surface charges on the polystyrene particles, contributing to their stability in suspension. It can also refer to the good capability of the presented polystyrene to capture cationic species.[25,26] After modification with ethanolamine, the

zeta potential charge remains negative. However, it shifted to a higher numerical value (−36.8 mV). This increased negative zeta potential value, compared to PS, is likely due to the present amine group in ethanolamine, which may coordinately interact with the surface of PS. Such interaction subsequently results in a negatively charged surface, owing to the presence of hydroxyl groups in the EA molecules.[27,28] The higher magnitude of the zeta potential, which suggests an improved colloidal stability, is explained by either an electrostatic interaction between amine and the hydroxyl groups or the occurrence of H-bonding between the EA molecules.[27,28] Upon the addition of Cr(OH)$_3$
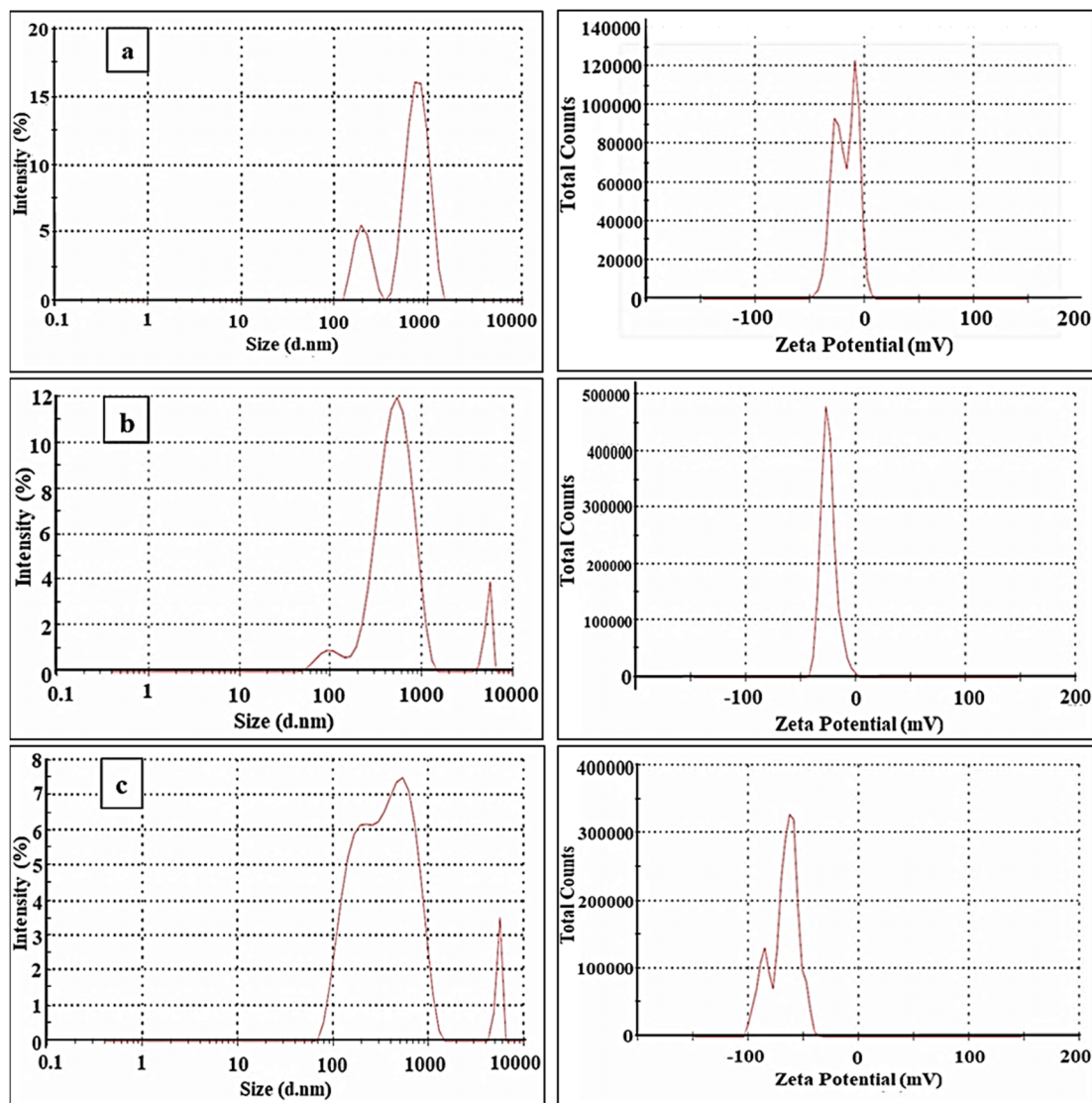
Fig. 4 DLS measurements and zeta potential curves of (a) polystyrene, (b) ethanolamine-blended polystyrene, (c) $Cr(OH)_3$-impregnated polystyrene/ethanolamine.

to the organic composite, a significantly higher negative zeta potential value of −76.6 mV was observed. This high negative value indicates the strong negative charge on the particle surfaces, which leads to excellent stability in the colloidal suspensions. This increased stability is because of the strong electrostatic repulsion between the particles, owing to the presence of numerous hydroxyl groups coming from both EA and the metal hydroxide molecules.[29,30] Thus, the introduction of additional functional groups in the two latter structures progressively increases their negative zeta potential values compared to blank PS.

In conclusion, it can be highlighted that the high magnitude of the zeta potential (either positive or negative) is generally desirable for colloidal stability since it prevents particle aggregation and sedimentation due to the strong electrostatic repulsion forces. Moreover, the highly negative zeta potential of a sample suggests its excellent potential for improved

adsorption and separation performance toward positively charged species due to its enhanced electrostatic interactions. Therefore, it can be expected that the final composite obtained *via* the combination of PS, EA and $Cr(OH)_3$ has strong potential as an adsorbent for heavy metal species.[27-30]

The three illustrated structures reveal different surface characteristics (Table 2), which appear to be strongly correlated with their final chemical components upon the consecutive

Table 2 Surface features of (a) polystyrene, (b) ethanolamine-blended polystyrene, (c) $Cr(OH)_3$-impregnated polystyrene/ethanolamine

Sample name	S_{BET} (m^2 g^{-1})	V_P (cm^3 g^{-1})	D_H (nm)
Blank PS	28.03	0.0418	2.605
EA-modified PS	17.28	0.0353	4.185
$Cr(OH)_3$-coupled EA/PS	53.46	0.0789	1.85

progression of the structure change. Both blank polystyrene and its subsequent composite achieved by blending with ethanol-amine showed mesoporous natures. However, a broader average pore diameter was observed for the blank PS. Accordingly, EA-modified PS displays lower specific surface area values and total pore volumes than those detected in the case of blank polystyrene. These variations can be explained by the blockage of some pores (especially those with small diameters) in PS by the EA particles during the process of producing the organic composite (EA-modified PS).[27,28] Therefore, the final surface area value of such composite and its total pore volume are reduced in comparison to blank polystyrene. Furthermore, by adding metal hydroxide particles to the organic composite, the obtained structure exhibits significant changes compared to either blank PS or EA/PS structures. In particular, the hybrid composite shows a microporous structure and a specific surface area value that is nearly double that observed for blank PS. Such composite displays the largest total pore volume among the investigated structures. These observations can be explained by the porous nature of the loaded metal hydroxide particles, which clearly increase the total pore volume in the sample. The metal hydroxide particles clearly change the average pore diameter of the composite due to their versatile pore diameter sizes, as well as their potential incorporation within some of the PS pores.[29,30]

3.2. Cadmium(II) adsorption studies

In this section, the tendency of the PS, EA-PS, and Cr@EA-PS sorbents for Cd(II) capture from aqueous solution is examined. The impacts of the main variables, such as the solution pH (1–5), contact time (5–600 min), sorbent dosage (1.0–5.0 g L^{-1}), and initial Cd(II) concentration (30–300 mg L^{-1}), on the sorption capacity were examined. Additionally, the sorption kinetics and isotherms were studied to explore the sorption characteristics of the applied polystyrene and the functionalized polystyrene structures.

3.2.1. Impact of pH. The influence of the solution pH on the Cd(II) adsorption process is illustrated in Fig. 5. As the

solution pH increased from 2.0 to 7.0, the sorption capacity increased from 0.3 to 0.9 mg g^{-1}, 0.4 to 1.0 mg g^{-1}, and 4.4 to 11.1 mg g^{-1} for PS, EA-PS, and Cr@EA-PS, respectively (Fig. 5). Conversely, the adsorption capacity decreased upon further increasing the solution pH. The performance of the prepared sorbents at different pH levels can be explained by the behavior of the Cd(II) ions in solution at different pH levels (Fig. S1†), and by the examination of the zeta potential for the utilized sorbent. The explored data reveal that the Cd(II) ions exhibit a divalent cationic species (Cd^{2+}) in a solution pH of ≤7, while the three applied sorbents reveal a negatively charged surface of −17.4, −36.8, and −76.6 mV for PS, EA-PS, and Cr@EA-PS, respectively (Fig. 4). This indicates that the electrostatic attraction between the cationic species and the negative sorbent surface will contribute effectively to the adsorption process. Nevertheless, at low solution pH, the high competition between the Cd^{2+} ions and the H$^+$ ions negatively affect the sorption capacity.[31,32] Additionally, the extra hydrogen ions cause the adsorbent's surface to become positively charged, which repels cations from the interface.[31,32] As the pH of the solution increases, the H$^+$ concentration decreases, enhancing the possibility for Cd(II) cations to interact with the active sites of the sorbent.[31,32] Beyond solution pH ≥ 7.0, the insoluble Cd(II) species (Cd(OH)$_2$) takes over as the dominant species, which lowers the adsorption affinity. A similar sorption performance (pH-dependent) was found for Cd(II) adsorption from aqueous solutions of compost derived from graphene oxide–silica composite,[33] Moroccan natural clays,[34] Bi/S co-doped carbon quantum dots,[35] and fruits and vegetables.[36]

3.2.2. Impact of the contact time and kinetic investigation. Fig. 6 illustrates the variation in the sorption capacity with respect to the contact time, which suggests that the Cd(II) uptake is a time-dependent process. The applied sorbents exhibit the same sorption performance (typical biphasic sorption performance). The accessibility of the sorbent surface active sites, which indicates a greater possibility of interaction with the cadmium(II) species, is attributed to the sorption
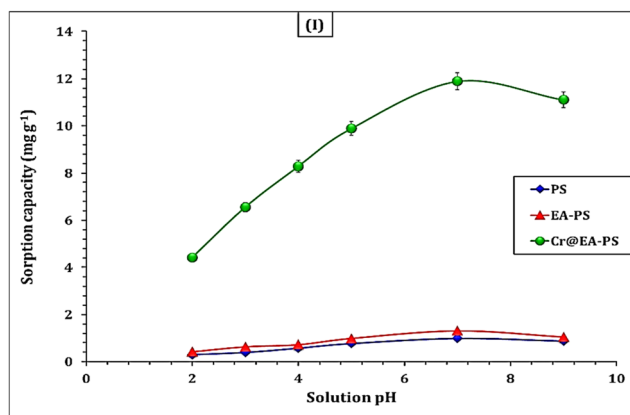

Fig. 5 The variation of Cd(II) sorption capacity as a function of pH (time: 240 min; room temperature; initial concentration: 50 mg L^{-1}; and sorbent dose: 3.0 g L^{-1}).

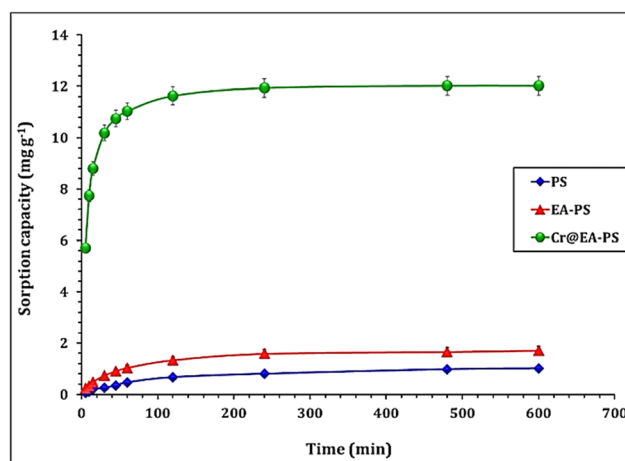**Fig. 6** Influence of the contact time on the Cd(II) adsorption capacity (pH 6.9; temperature of 25 ± 1 °C; initial concentration of 50 mg L^{-1}; sorbent dosage of 3.0 g L^{-1}).

percent rise in the initial part as the reaction time progresses until it reaches the equilibrium period (240 min).[31,32] Furthermore, the external resistance caused by the Cd(II) species approaching each other is successfully overcome by the force generated from the concentration gradient.[31,32] Notably, Cr@EA-PS possesses the highest sorption tendency with regards to Cd(II) ions, while PS displays the lowest affinity for Cd(II) ions. The highest sorption capacities of the PS, EA-PS, and Cr@EA-PS sorbents at equilibrium are approximately 1.2, 1.8 and 12.1 mg g^{-1}, respectively. After the equilibrium time, the reaction time (second stage), which is controlled by the sorbent surface functional groups' fullness, has a minor impact on the sorption effectiveness.[37,38] Therefore, the intra-diffusion mechanism takes place alongside electrostatic repulsion between the Cd(II) cationic species when the equilibrium time is exceeded, occupying most of the active sites at the surfaces of the compounds. Therefore, they potentially migrate away from the particles of the composites, leading to stable activities toward the adsorption of cadmium(II) ions.[37,38] Other studies, such as those on Cd(II) adsorption from aqueous solution by graphene oxide–silica composite,[33] Moroccan natural clays,[34] Bi/S co-doped carbon quantum dots,[35] and fruits and vegetables are previously reported through literature survey.[36]

The kinetics of Cd(II) uptake using the PS, EA-PS, Cr@EA-PS sorbents was explored by analyzing the change in the adsorption capacity (q_t) over the time interval of 5–600 min using pseudo-first-order (PFO) and pseudo-second-order (PSO) kinetic models.[38–40] The main concept of each model is explained in the corresponding references. The nonlinear equations for each model are given in Table S1.†[38–40] The fitting of the models is determined using the equations of the average relative error (ARE) and Chi-square coefficient (x^2) (Table S1†).[25,26] Fig. 7(I–III) displays the kinetic profile of the PS, EA-PS, Cr@EA-PS sorbents, respectively. The anticipated results demonstrate that the applied sorbents show similar kinetic profiles, but with different magnitudes. Initially, the adsorption capacity quickly increases (fast rate of reaction) and remains that way up to 240 min (the equilibrium point), owing to the presence of free sorbent active sites at the beginning of the adsorption process. With the extended equilibrium state, the majority of the surface functional groups binds to the metal ions; therefore, the adsorption capacity essentially stays constant (flat shape).[31,32]

The gathered values of the kinetic terms (Table 3) show that the pseudo-second-order model had the lowest average relative error and Chi-square coefficient, indicating that it fits well with the adsorption process. This suggests that the uptake of Cd(II) is a chemisorption process, and that an electron sharing or transfer process occurs during the interaction between the Cd(II) ions and the prepared sorbents.[38–40] The adsorption capacity of the applied sorbents towards Cd(II) ions is ranked as PS < EA-PS < Cr@EA-PS, which reflects the modification of the polystyrene with ethanolamine and the improvement of the sorption characteristics of the polystyrene by chromium hydroxide. Similar kinetic performance (chemisorption uptake process) was recognized for Cd(II) adsorption from aqueous solution by composites derived from a graphene oxide–silica
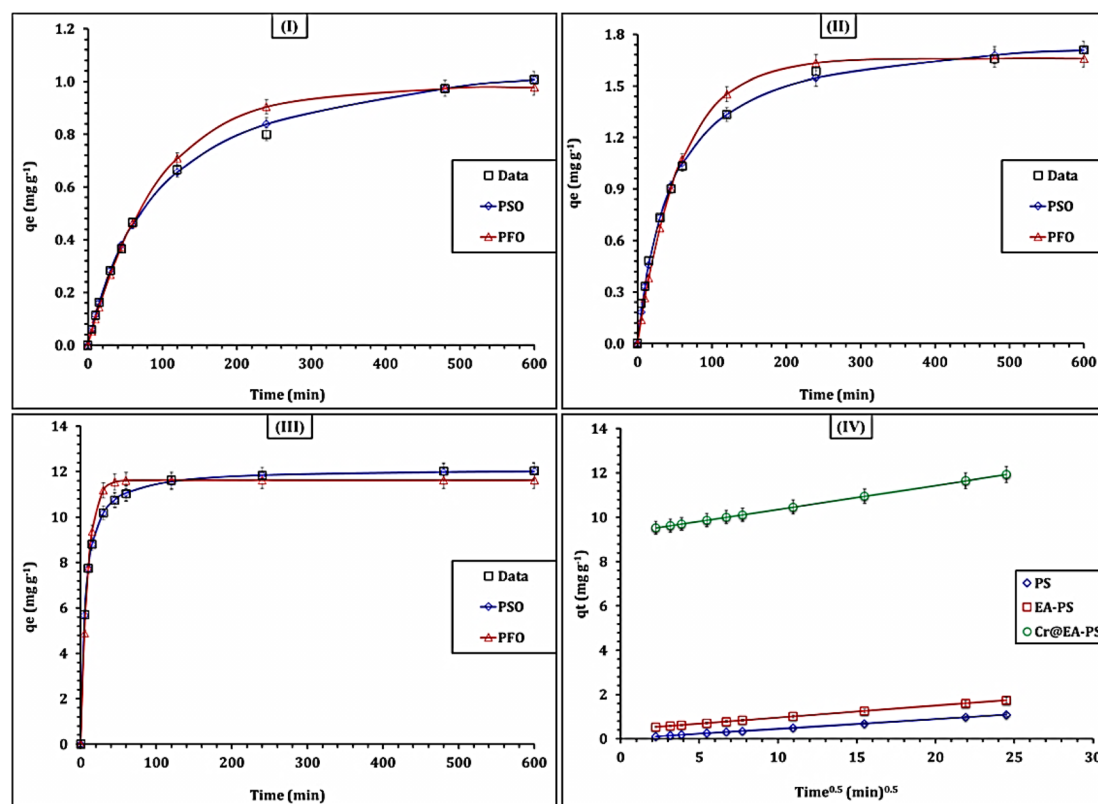

Fig. 7 The kinetic illustration of PS (I), EA-PS (II), and Cr@EA-PS (III) materials. The IPA for the three sorbents (IV).

Table 3 The values of the applied kinetics model parameters

	PS	EA-PS	Cr@EA-PS
Pseudo first-order model			
q_1 (mg g^{-1})	1.0	1.7	11.6
k_1 (min^{-1})	0.011	0.017	0.109
ARE	6.9	11.0	5.2
X^2	0.02	0.13	0.42
Pseudo second-order model			
q_2 (mg g^{-1})	1.2	1.8	12.1
k_2 (min^{-1})	0.009	0.012	0.014
h (mol g^{-1} h^{-1})	0.01	0.04	2.13
$t_{1/2}$ (h)	92.6	45.1	5.7
ARE	1.4	3.4	0.3
X^2	0.02	0.02	0.02

composite,[33] Moroccan natural clays,[34] Bi/S co-doped carbon quantum dots,[35] and fruits and vegetables.[36]

Notably, the rate constant of Cr@EA-PS is the highest among the applied sorbents (0.014 min^{-1}), followed by EA-PS (0.012 min^{-1}). However, the lowest reaction rate belongs to PS (0.009 min^{-1}). In addition, Cr@EA-PS has the highest initial adsorption rate (2.13 mol g^{-1} h^{-1}), followed by EA-PS (0.04 mol g^{-1} h^{-1}), while PS has the lowest initial adsorption rate (0.01 mol g^{-1} h^{-1}). Conversely, the half-equilibrium time has the following order: PS > EA-PS > Cr@EA-PS. These findings confirm that the Cr@EA-PS sorbent possesses the highest affinity towards Cd(II) ions, followed by EA-PS, while the lowest affinity belongs to the PS sorbent. These findings are consistent with the gained experimental results.

This attribute is due to the variation in the surface area, pore volume, and particle size between the three applied sorbents, whereas Cr@EA-PS possesses the lowest particle size (Fig. 4), and the highest surface area and pore volume (Table 2). Furthermore, Cr@EA-PS exhibits the highest zeta potential value, which reflects its greater colloidal stability and higher tendency to interact statically with the Cd(II) cationic species. This reflects that the PS activation using EA and Cr(OH)$_3$ improves the surface properties, and in turn the sorption characteristics. Moreover, the activation using cobalt metal is more effective than that achieved with nickel metal. The detailed Cd(II) adsorption mechanisms are deduced in Section 3.2.

In general, the adsorption capability depends on the sorbent physicochemical properties.[39,40] Adsorption may take place due to physical, chemical, or both physical and chemical reactions on the surface of the adsorbents. Physical adsorption may occur *via* a porous structure, and chemical adsorption occurs *via* surface functional groups.[39,40] Physical adsorption is controlled by intraparticle diffusion or liquid film diffusion. Thus, the adsorption mechanism of Cd(II) can be thoroughly examined by analyzing the data using the Weber–Morris model.[41] The plot of the diversity of sorption capacity against time$^{0.5}$ (Fig. 7-IV) exhibits the Weber–Morris model. The attained values of the kinetic parameters are summarized in Table S2.†

The attained results indicate that the three sorbents show proper straight lines however without passing through the

origins. This indicates that there are several interaction mechanisms controlling the adsorption process. From the terms of the W–M equation (Table S2†), the three materials display a good correlation coefficient ($R^2 = 0.99$), which reveals that the Cd(II) adsorption process is controlled *via* multiple mechanisms (*i.e.*, chemical and physical mechanisms).[39–41] This indicates that the chemical mechanisms, such as complexation mechanism, control the uptake process at the initial stage of the process and extend up to the equilibrium stage. With extended equilibrium, physical mechanisms (*i.e.*, intra-particular diffusion of Cd(II) ions into the sorbent pores) take place through a physisorption interaction mechanism.[39–41] In addition, the Cr@EA-PS material exhibits the highest reaction rate ($K_i = 0.11$ mg g^{-1} min$^{-1/2}$), followed by EA-PS ($K_i = 0.05$ mg g^{-1} min$^{-1/2}$), and then polystyrene polymer ($K_i = 0.04$ mg g^{-1} min$^{-1/2}$), indicating that Cr@EA-PS possesses the highest affinity towards Cd(II) ions.

3.2.3. Impact of the sorbent dose. One important factor that regulates the adsorption system is the sorbent dosage, which is indicative of the effective surface area. Within the increase in the sorbent dose from 1.0 to 5.0, as Fig. 8-I illustrates, the adsorption capacity of the Cd(II) ions is decreased from 1.0 to 0.7 mg g^{-1} for PS, from 1.5 to 1.2 mg g^{-1} for EA-PS, and from 14.3 to 8.2 mg g^{-1} for Cr@EA-PS. As the sorbent dose is increased, the particles begin to overlap and coat one another, which limits the available surface area and the accessibility of active sites, lowering the q_e value.[25,26] Furthermore, the excess sorbent active sites become disproportionate to the relatively low concentration of Cd(II) ions in the solution, further reducing the adsorption efficiency at higher dosages.[25,26] Even though the efficiency per unit mass (q_e) decreases, the uptake efficiency improves from 2.1% to 7.3%, 3.1% to 11.8%, and 28.7% to 81.9% for PS, EA-PS, and Cr@EA-PS, respectively, within the same increase in the sorbent dose. The increased surface area and subsequent number of active sites resulting from an increase in the sorbent dose can be used to explain this phenomenon, and improve the adsorption capacity.[25,26] As shown in Fig. 8-II, the calculated K_d values from the Cd(II) removal experiment are significantly varied with the change of sorbent dose, confirming its complex interactions between metol ions and the surface functional group of the sorbent.[31,32] The functionalization of PS with ethanolamine (EA-PS) and the impregnation with chromium oxide (Cr@EA-PS) enhance these interactions, leading to better Cd(II) capture. The improvement in K_d values supports the enhanced binding affinity of the sorbents, particularly for Cr@EA-PS, due to the increased number of active functional groups available for interaction with the Cd(II) ions.

3.2.4. Impact of Cd(II) initial concentration and isotherm investigation. The dependence of the Cd(II) adsorption capacity for the PS, EA-PS, Cr@EA-PS sorbents on the Cd(II) starting concentration interval of 30–300 mg L^{-1} is displayed in Fig. 9. The findings show that all three materials exhibit comparable sorption attributes. At low Cd(II) concentration, the sorption affinity improves, which is thought to be because the sorbent active sites are more readily obtained.[37,38] However, because of the saturation of the sorbent active sites, the sorption tendency
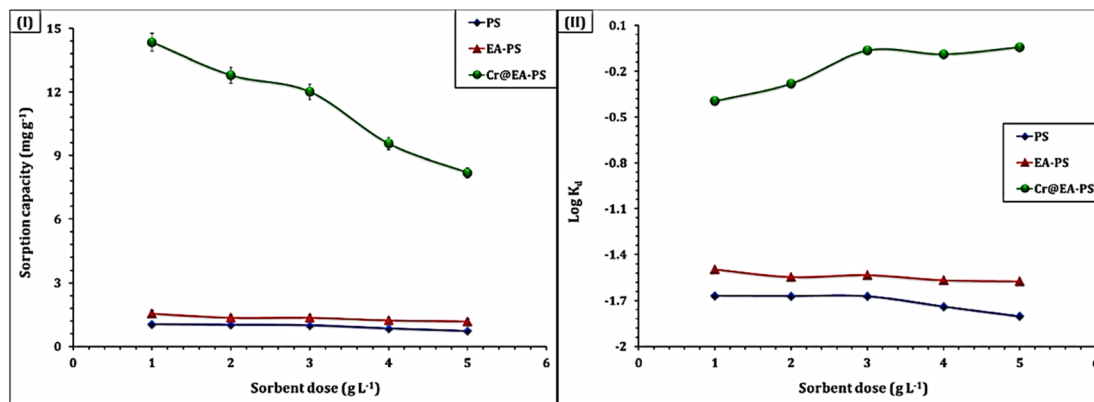
Fig. 8 The dependence of sorption capacity (I) and the distribution coefficient ($\log K_d$) (II) on the sorbent dose (room temperature; initial concentration of 50 mg L^{-1}; time of 240 min; solution pH 6.9).
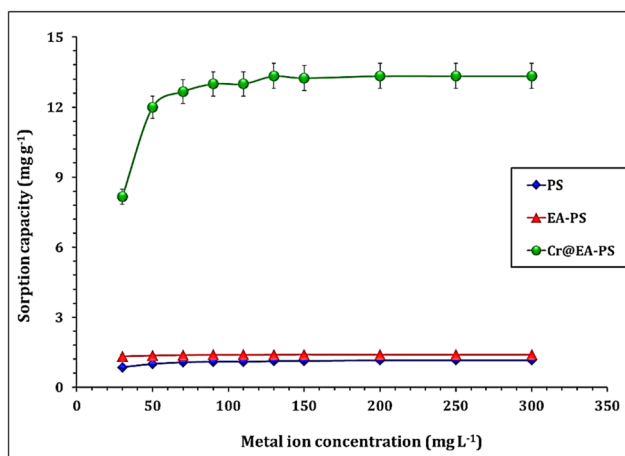

Fig. 9 Influence of metal ion initial concentration on the Cd(II) adsorption capacity (temperature of 25 ± 1 °C; pH 7.0; sorbent dosage of 3.0 g L; time is 240 min).

is slightly altered at high Cd(II) starting concentration.[37,38] A similar performance was observed when graphene oxide–silica composite,[33] Moroccan natural clays,[34] and Bi/S co-doped carbon quantum dots[35] were applied for Cd(II) uptake from aqueous solution. Fig. 9 visually confirms the superior performance of Cr@EA-PS, showing a steeper initial slope and a higher plateau, which are indicative of both stronger affinity and higher capacity for cadmium(II) adsorption across the entire studied concentration range. The improvement in the adsorption properties with the addition of ethanolamine and metal oxide to polystyrene is a significant finding.

The isotherm performance and the maximum capacity were explored by modeling the test results using the Langmuir, Freundlich, Dubinin–Radushkevich (D–R) and Sips isotherm models. The references used to develop these models are mentioned in the study.[42–44] The equations used in the models are provided in Table S1.†[42–44] The fitting of the models was evaluated using the average relative error (ARE) and Chi-square coefficient (X^2) equations (Table S1†).[25,26] The sorption capacity (q_e) of Cd(II) is plotted against the residual concentration

(isotherm curve) in Fig. 10, while the values of the isotherm variables are provided in Table 4.

The anticipated results confirm that the three sorbents exhibit the same isotherm profile (Type I isotherm), which is characterized by a rapid boost in the adsorption capacity with the increment of the starting concentration up to saturation; *i.e.*, they have a partially or completely horizontal plateau.[42,43] This performance is typical for porous materials. The displayed results in Table 4 reveal that the Langmuir isotherm model has the lowest average relative error and Chi-square coefficients. This indicates that the adsorption nature is uniform and homogeneous.[25,26] The highest capacity (q_m) for the PS, EA-PS, Cr@EA-PS sorbents towards the Cd(II) ions is approximately 1.2, 1.4, and 13.6 mg g^{-1}, respectively. This means that the affinity of the sorbents towards the Cd(II) ions is ranked as Cr@EA-PS > EA-PS > PS, which is consistent with the findings from kinetic analysis. This performance is attributed to the improvement of the surface properties of PS by the activation process using ethanolamine and metal oxides, as discussed in Section 3.2.2.

The sequential enhancement in the adsorption capacity observed from PS to EA-PS to Cr@EA-PS can be attributed to the incremental modifications in the surface chemistry and morphological characteristics through each addition to the PS structure. The functionalization with amine groups in EA-PS facilitates enhanced chemisorption *via* surface complexation mechanisms. Subsequently, the incorporation of Cr(OH)$_3$ in Cr@EA-PS results in a higher density of active adsorption sites and introduces supplementary uptake pathways, notably surface precipitation phenomena at elevated Cd(II) concentrations.

The process of Cd(II) adsorption is favorable, which is evident from the dimensionless equilibrium term $R_L = (1/(1+K_L \times C_0))$. If the value of R_L is between zero and one, then the process is favorable. On the other hand, if R_L is greater than one, then the process is unfavorable.[25,26] According to the data presented in Fig. 10-IV, the R_L values were between zero and one for the three sorbents, indicating a favorable adsorption process. A similar isotherm performance was observed in various studies,
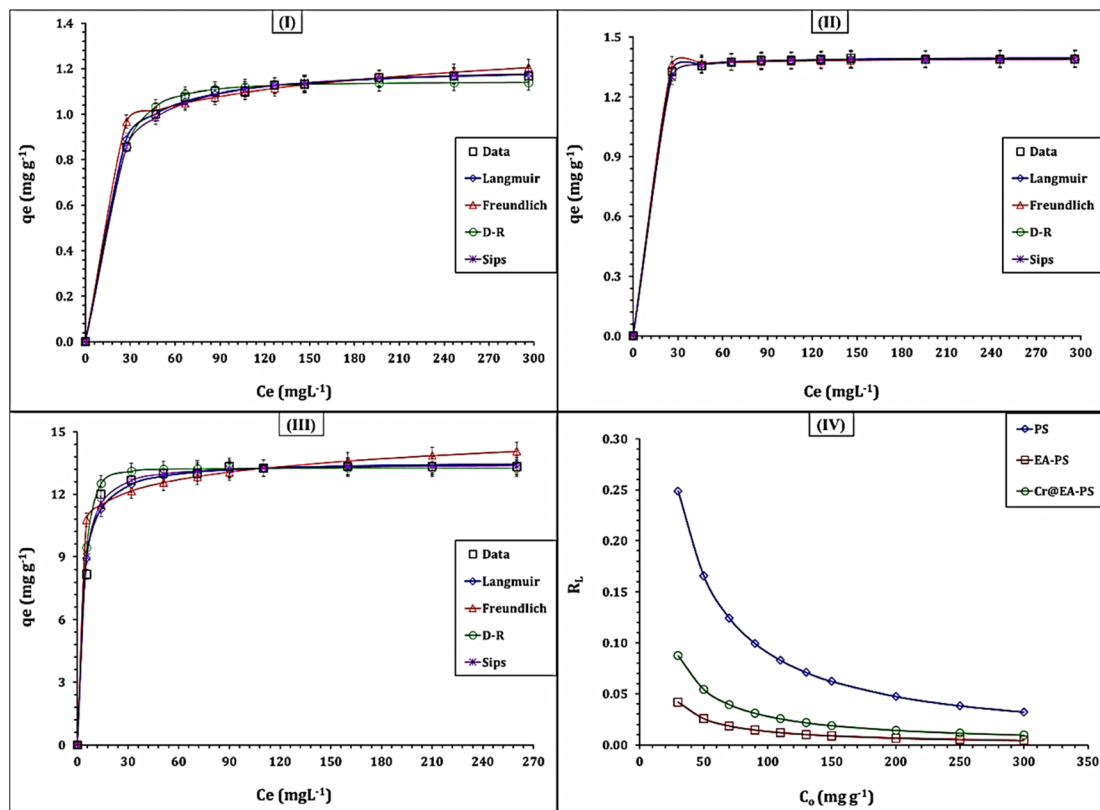
© 2025 The Author(s). Published by the Royal Society of Chemistry

Fig. 10 The isotherm profile of PS(I), EA–PS(II), and Cr@EA–PS(III) materials. The dimensionless R_L values for the three sorbents (IV).

Table 4 The values of the applied isotherm model parameters

	PS	EA-PS	Cr@EA-PS
Langmuir model			
q_m (mg g^{-1})	1.2	1.4	13.6
k_L (L mg^{-1})	0.10	0.76	0.35
ARE	0.9	0.3	2.1
X^2	0.01	0.01	0.12
Freundlich model			
$1/n_F$	0.09	0.01	0.07
k_F (mg g^{-1}) (mg L^{-1})	0.71	1.32	9.58
ARE	2.6	0.6	5.8
X^2	0.02	0.02	0.76
D–R model			
q_D (mg g^{-1})	1.1	1.4	13.3
B (mol^2 kJ^{-2})	36.6	7.6	2.0
E_{ad}	0.1	0.3	0.5
ARE	1.4	0.4	2.9
X^2	0.02	0.02	0.22
Sips model			
q_S (mg g^{-1})	1.2	1.4	13.4
k_S (L mg^{-1})	0.08	0.13	0.33
m_S	1.1	2.2	1.2
ARE	0.8	0.3	1.7
X^2	0.01	0.01	0.01

such as the adsorption of Cd(II) from aqueous solution by compost derived from graphene oxide–silica composite,[33] Moroccan natural clays,[34] Bi/S co-doped carbon quantum dots,[35] and fruits and vegetables.[36] These studies all demonstrated a monolayer, uniform, and homogeneous adsorption process.

The Sips isotherm model combines the Freundlich and Langmuir models to predict the adsorption process. It is useful for heterogeneous adsorption at low adsorbate concentrations, and reduces to the Langmuir isotherm model at high concentrations.[42–44] The results from Table 4 show that the Sips model fits the experimental results with low ARE and X^2 coefficients. As per the Sips model, the q_S and q_m values are the same with a maximum sorption capacity of 1.2, 1.4, and 13.4 mg g^{-1} for the Cr@EA-PS, EA-PS, and PS sorbents, respectively. This is consistent with the results from the Langmuir model. It is worth noting that the Sips constant (k_S) for Cr@EA-PS (0.33 L mg^{-1}) > EA-PS (0.13 L mg^{-1}) > PS (0.08 L mg^{-1}) confirms the higher affinity of the Cr@EA-PS sorbent.

The Freundlich isotherm model has suitable ARE and X^2 coefficients, indicating that the three sorbents can effectively uptake Cd(II) even at low initial concentrations. It suggests that the Cd(II) uptake process is predominantly a monolayer process, with a slight contribution from the multi-layer adsorption process.[42–44] The adsorption intensity ratio, $1/n_F$, can be used to determine the profile of the Cd(II) adsorption process. If $1/n_F$ is less than one, the process is favorable, and if it is greater than one, the process is unfavorable.[42–44] The data in Table 4 show

that $1/n_F$ is < 1.0 for the three sorbents, indicating the favorability of the Cd(II) uptake process.

The Dubinin–Radushkevich model, which follows the pore-filling mechanism, suggests that a multilayer adsorption process through van der Waal's forces occurs during the Cd(II) ions adsorption process.[42–44] This is supported by the ARE and X^2 coefficient values. The maximum sorption capacity (q_{ad}) was found to be 1.1 and 1.3, and 13.3 mg g^{-1} for the Cr@EA-PS, EA-PS, and PS sorbents, respectively, which is close to the maximum sorption capacity calculated from the Langmuir and Sips models. The mean free energy (E_{ad}, kJ mol^{-1}) can be used to determine the nature of the sorption process. $E < 8$ kJ mol^{-1} reflects a physisorption process, whereas $8 < E < 16$ kJ mol^{-1} indicates a chemisorption process.[42–44] In this case, the data in Table 4 suggest a physisorption process (through van der Waals force) since $E \leq 0.5$ kJ mol^{-1}.

In summary, the inferences from the isotherm studies are consistent with the outcomes from the W–M kinetic model, whereas the adsorption of Cd(II) ions is controlled by multiple reaction mechanisms (*i.e.*, chemisorption mechanisms as revealed from the Langmuir model, with a significant contribution for the physisorption mechanisms as shown from the D–R model).

Table 5 shows the sorption capacity of the three carbonaceous sorbents for Cd(II) ions, with a comparison to other sorbents in the literature. The results show that the present Cr@EA-PS offers a balanced trade-off between performance, cost, and ease of synthesis, providing a sustainable solution for Cd(II) removal from water by balancing the proper adsorption efficiency with practical advantages over both natural and advanced adsorbents.

3.2.5. Proposed adsorption mechanism. Understanding cadmium–sorbent interaction mechanisms is crucial for providing valuable insights into optimizing these sorbents for practical applications in Cd(II) removal from aqueous solutions. Adsorption of cadmium(II) ions from aqueous solutions can involve multiple mechanisms, including surface complexation,

electrostatic attraction, ion exchange, precipitation, and physical sorption through mesopore filling.[31,37,52–55] These mechanisms are primarily governed by cadmium speciation in the aqueous solution and the physicochemical properties of the adsorbent material, such as chemical composition, pore structure, and surface area.[31,37,54,55] Recent studies have demonstrated that the precipitation of metal ions with minerals contained in bio-char is the dominant mechanism for metal ion sorption.[53] However, other studies have suggested that the cation exchange mechanism and surface complexation between metal ions and the oxygen-containing functional groups of bio-char are also significant factors.[31,37,55,56] Additionally, the cation–π interaction mechanism is involved in metal ion sorption using bio-chars with highly cyclic aromatic structures, and the bio-char can be used as a π-donor.[55,56] Conversely, the electrostatic attraction mechanism is expected for metal ion sorption using biochar with pH$_{pzc}$ < solution pH, where the bio-char surface becomes negatively charged and is attracted to positively charged cation species.[37,57] The large surface area and suitable micropore structure of biochar enhance the contribution of the physical adsorption mechanism for removing metal ions from an aqueous solution.[55,56]

In the current study, the adsorption of Cd(II) ions onto PS, EA-PS, and Cr@EA-PS is a complex and multi-step process influenced by the sorbents' surface chemistry, morphology, and textural properties, as well as the speciation of Cd(II) in solution. The mechanisms involve physical adsorption, electrostatic interactions, ion exchange, surface complexation, and potential precipitation at higher concentrations. Electrostatic interactions play a significant role in the initial stages of adsorption. Zeta potential analysis reveals that all three sorbents (PS, EA-PS, and Cr@EA-PS) exhibit negatively charged surfaces, with values becoming increasingly negative from PS (−17.4 mV) to EA-PS (−36.8 mV) to Cr@EA-PS (−76.6 mV) (Fig. 4).[37,57] Given that Cd(II) exists predominantly as a cationic species in the studied pH range (Fig. S1†), these negative surface charges promote strong electrostatic attractions, particularly for EA-PS and

Table 5 Comparison of sorption performance of Cd(II) for different sorbents

Sorbent	Time, min	Temp., °C	C_0, mg L^{-1}	pH	q_e, mg g^{-1}	R
Meso iron oxyhydroxide impregnated bead	1440	25	1–50	4	9.9	45
Compost derived from fruits and vegetables	1140	28	5–60	6	6.35	36
Treated laterite	1440	25	20–60	7	3.7	46
Buckthorn leaves	180	25	0.1–10	6	0.208	47
Moroccan clays (QC-MT)	45	25	5–120	5	5.85	34
Graphene oxide–silica composite	100	25	40–80	6	43.45	33
Bombax ceiba fruit shell-activated carbon	180	25	5–30	9	4.37	48
Bentonite/TiO$_2$	480	25	3–12	7	13.14	49
Processed walnut shell	30	25	1–200	5	11.56	50
Chemically modified chitin with polypyrrole	120	30	10–20	6	6.17	51
PS	240	25	30–300	7	1.1	PW
EA-PS					1.3	
Cr@EA-PS					13.3	

Cr@EA-PS. Surface complexation is another crucial mechanism, especially for EA-PS and Cr@EA-PS. FTIR analysis (Fig. 1) confirms the presence of amine groups in EA-PS and hydroxyl groups in Cr@EA-PS, which can form inner–sphere complexes with Cd(II) ions.[55,56] This chemisorption process is consistent with the good fit of the pseudo-second-order kinetic model. The XRD-confirmed presence of crystalline $Cr(OH)_3$ in Cr@EA-PS (Fig. 2) provides additional sites for surface complexation and potential ion exchange with Cr^{3+}. The cation-π interactions mechanism may also contribute to Cd(II) adsorption, particularly in PS and EA-PS, due to their aromatic structures acting as π-donors.[55,56] This mechanism can explain the adsorption capacity of PS, despite its relatively smooth surface and lower negative charge.

Physical sorption and intraparticle diffusion become more significant as the sorption process progresses. The SEM images (Fig. 3) reveal increasing surface roughness and porosity from PS to EA-PS to Cr@EA-PS, providing larger surface areas and more diverse adsorption sites.[31,37,54,55] The Weber–Morris kinetic model results suggest that while chemisorption is the initial dominant mechanism, physisorption mechanisms such as intraparticle diffusion become more prominent after the equilibrium stage (Fig. 7). This is further supported by the observed decrease in surface area values post-adsorption and the good fit of the D–R isotherm model, which indicates contributions from both chemisorption and physisorption processes (Table 4).

The progressive enhancement in the adsorption capacity from PS to EA-PS to Cr@EA-PS can be attributed to the increasing complexity of the surface chemistry and morphology. The introduction of amine groups in EA-PS enhances chemisorption through surface complexation. The impregnation with $Cr(OH)_3$ in Cr@EA-PS further increases the available adsorption sites, and introduces additional mechanisms such as surface precipitation at higher Cd(II) concentrations.

In conclusion, the adsorption of Cd(II) onto these modified polystyrene sorbents involves a synergy of mechanisms. It begins with rapid electrostatic attractions and surface complexation, followed by slower processes, including intraparticle diffusion and potential multilayer adsorption at higher concentrations. The balance between these mechanisms shifts from predominantly physisorption in PS to a more chemisorption-dominated process in EA-PS and Cr@EA-PS, explaining their enhanced performance.

3.2.6. Investigation of desorption and recycling process. The efficacy of the adsorption process and its potential for practical application heavily depend on the sorbent's ability to undergo desorption and be reused multiple times. To evaluate these crucial aspects, desorption and recycling studies were conducted on the Cr@EA-PS sorbent, which had demonstrated the highest sorption efficiency for Cd(II) ions. Desorption experiments were performed using three different mineral acids: hydrochloric (HCl), nitric (HNO$_3$), and sulfuric (H$_2$SO$_4$). The experimental conditions were standardized across all tests, with an acid concentration of 1.0 M, room temperature, a shaking time of 240 min, and a sorbent dosage of 3.0 g L^{-1}. The results reveal a clear hierarchy in the effectiveness of these acids for Cd(II) desorption. Hydrochloric acid

(HCl) showed the highest desorption efficiency at 93.8%. Nitric acid (HNO$_3$) demonstrated moderate effectiveness with 78.2% desorption. Sulfuric acid (H$_2$SO$_4$) proved to be least effective, achieving only 64.7% desorption.

To assess the sorbent's reusability, five consecutive adsorption–desorption cycles were conducted. Before each cycle, the sorbent was washed with deionized water to remove any residual acid. The results demonstrate the Cr@EA-PS sorbent's robustness and potential for repeated use, as shown in Table S3.† The initial adsorption capacity was 12.0 mg g^{-1}, with a corresponding desorption efficiency of 93.4%. Over five cycles, there was a gradual decrease in both adsorption and desorption efficiencies. By the fifth cycle, the adsorption capacity had decreased to 11.7 mg g^{-1}, while the desorption efficiency dropped to 90.4%. The observed decline in performance over multiple cycles is relatively minor, with only a 2.5% decrease in the adsorption capacity and a 3% reduction in the desorption efficiency. This minimal loss in effectiveness suggests that the Cr@EA-PS sorbent maintains its structural integrity and functional properties well, even after repeated use and exposure to acidic conditions.

These findings highlight the Cr@EA-PS sorbent's potential for practical applications in Cd(II) removal from aqueous solutions. Its high desorption efficiency with HCl and sustained performance over multiple cycles indicate that it may be a cost-effective and environmentally-friendly option for water treatment processes, particularly in scenarios requiring repeated use of the sorbent material.

4. Conclusion

The modification of polystyrene with ethanolamine and the subsequent impregnation of chromium hydroxide significantly enhance the sorption characteristics of the final produced composite toward Cd(II) ion removal. The characterization of the sorbents revealed that these modifications introduced critical functional groups and improved surface features for this composite, enhancing its adsorption capability due to the presence of additional active sites. Kinetic and isotherm analyses confirmed that the adsorption process involved both chemisorption and physisorption, with the Cr@EA-PS sorbent demonstrating the highest adsorption capacity and fastest adsorption rate. The superior performance of Cr@EA-PS was attributed to the synergistic effects of ethanolamine functionalization and chromium hydroxide impregnation, which facilitated electrostatic interactions and complexation with Cd(II) ions. Furthermore, Cr@EA-PS exhibited remarkable stability for sorption/desorption over five successive cycles. These findings suggest that Cr@EA-PS has significant potential for use in cost-effective and environmentally sustainable water treatment applications, offering a promising approach to remove toxic heavy metals from contaminated water sources.

Data availability

All the utilized data are presented in the manuscript. However, any other required data will be made available upon request.

Author contributions

Conflicts of interest

The authors of this article would like to confirm that there are no conflicts of interests with any organization or any person, and the funding body is listed.

Acknowledgements

References

1 A. M. Elgarahy, H. Y. Mostafa, E. G. Zaki, S. M. Elsaeed, K. Z. Elwakeel, A. Akhdhar and E. Guibal, International Journal of Biological Macromolecules Methylene blue removal from aqueous solutions using a biochar/gellan gum hydrogel composite : effect of agitation mode on sorption kinetics, *Int. J. Biol. Macromol.*, 2023, **232**, 123355, DOI: **10.1016/j.ijbiomac.2023.123355**.

2 S. K. R. Yadanaparthi, D. Graybill and R. von Wandruszka, Adsorbents for the removal of arsenic, cadmium, and lead from contaminated waters, *J. Hazard. Mater.*, 2009, **171**, 1–15, DOI: **10.1016/j.jhazmat.2009.05.103**.

3 N. A. A. Qasem, R. H. Mohammed and D. U. Lawal, Removal of heavy metal ions from wastewater: a comprehensive and critical review, *npj Clean Water*, 2021, **4**(1), 1–15, DOI: **10.1038/s41545-021-00127-0**.

4 S. N. I. S. Najamuddin, N. M. Shukri, N. F. M. Salleh, W. N. W. Abdullah, N. A. M. Shohaimi, A. Z. Ab Halim and N. H. Abdullah, Simultaneous Removal of Lead, Cadmium, and Arsenic Ions from Bivalve Species Using Adsorption Method, *IOP Conf. Ser.: Earth Environ. Sci.*, 2022, **1102**(1), 012013, DOI: **10.1088/1755-1315/1102/1/012013**.

5 Z. Peng, D. Zhao, J. Fang, J. Chen and J. Zhang, Biosynthetic amyloid fibril CsgA-Fe₃O₄ composites for sustainable removal of heavy metals from water, *Sep. Purif. Technol.*, 2024, **329**, 125191, DOI: **10.1016/j.seppur.2023.125191**.

6 J. Zhou, Y. Liu, B. Li, H. Li, G. Chen and R. Qiu, Coagulation of trace arsenic and cadmium from drinking water using titanium potassium oxalate, *npj Clean Water*, 2023, **6**, 1–10, DOI: **10.1038/s41545-023-00227-z**.

7 Y. Wu, Y. Zhao, Z. Xu, R. Wang, H. Zhang, S. Feng and J. Guo, Efficient Removal of Cadmium (II) and Arsenic (V) from Water by the Composite of Iron Manganese Oxides Loaded Muscovite, *Water*, 2023, **15**(20), 3579, DOI: **10.3390/w15203579**.

8 M. S. Fernando, A. K. D. V. K. Wimalasiri, K. Dziemidowicz, G. R. Williams, K. R. Koswattage, D. P. Dissanayake, K. M. N. De Silva and R. M. De Silva, Biopolymer-Based Nanohydroxyapatite Composites for the Removal of Fluoride, Lead, Cadmium, and Arsenic from Water, *ACS Omega*, 2021, **6**, 8517–8530, DOI: **10.1021/acsomega.1c00316**.

9 H. Chen, F. Xu, Z. Chen, O. Jiang, W. Gustave and X. Tang, Arsenic and cadmium removal from water by a calcium-modified and starch-stabilized ferromanganese binary oxide, *J. Environ. Sci.*, 2020, **96**, 186–193, DOI: **10.1016/j.jes.2020.03.060**.

10 M. Luo, H. Lin, Y. He, B. Li, Y. Dong and L. Wang, Efficient simultaneous removal of cadmium and arsenic in aqueous solution by titanium-modified ultrasonic biochar, *Bioresour. Technol.*, 2019, **284**, 333–339, DOI: **10.1016/j.biortech.2019.03.108**.

11 S. S. Alquzweeni and R. S. Alkizwini, Removal of Cadmium from Contaminated Water Using Coated Chicken Bones with Double-Layer Hydroxide (Mg/Fe-LDH), *Water*, 2020, **12**(8), 2303, DOI: **10.3390/w12082303**.

12 I. Suhani, S. Sahab, V. Srivastava and R. P. Singh, Impact of cadmium pollution on food safety and human health, *Curr. Opin. Toxicol.*, 2021, **27**, 1–7.

13 H. R. Ali, H. Y. Mostafa, S. Husien and A. N. El-hoshoudy, Adsorption of BTX from produced water by using ultrasound-assisted combined multi-template imprinted polymer (MIPs); factorial design, isothermal kinetics, and Monte Carlo simulation studies, *J. Mol. Liq.*, 2023, **370**, 121079, DOI: **10.1016/j.molliq.2022.121079**.

14 M. Kaur, N. Sidhu and M. S. Reddy, Removal of cadmium and arsenic from water through biomineralization, *Environ. Monit. Assess.*, 2023, **195**, 1–19, DOI: **10.1007/s10661-023-11616-9**.

15 A. M. Mahmoud, A. A. Ali, M. Alshukur, M. E. Sultan, H. Y. Mostafa, E. A. Eldeeb and A. M. Ashmawy, Novel kappa-carrageenan – poly (vinyl alcohol) – modified pumice hydrogel composite for the adsorption of cationic dye, Egypt, *J. Chem.*, 2023, **66**, 21–35, DOI: **10.21608/ejchem.2023.176082.7210**.

16 C. Sabando-Fraile, M. Corral-Bobadilla, R. Lostado-Lorza and F. Gallarta-González, Applying circular economy principles and life cycle assessment: a novel approach using vine shoots waste for cadmium removal from water, *Sci. Total Environ.*, 2024, **926**, 171947, DOI: **10.1016/j.scitotenv.2024.171947**.

17 M. Alshabanat, Removal of heavy metal ions using polystyrene nanocomposite thin films, Egypt, *J. Chem.*, 2019, **62**, 149–156, DOI: **10.21608/EJCHEM.2018.4056.1354**.

18 G. Chen, C. Wang, J. Tian, J. Liu, Q. Ma, B. Liu and X. Li, Investigation on cadmium ions removal from water by different raw materials-derived biochars, *J. Water Process Eng.*, 2020, **35**, 101223, DOI: **10.1016/j.jwpe.2020.101223**.

19 A. Thakur, A. Kumar and A. Singh, Adsorptive removal of heavy metals, dyes, and pharmaceuticals: carbon-based

nanomaterials in focus, *Carbon*, 2024, **217**, 118621, DOI: 10.1016/j.carbon.2023.118621.

20 B. S. Barus, K. Chen, M. Cai, R. Li, H. Chen, C. Li, J. Wang and S. Y. Cheng, Heavy Metal Adsorption and Release on Polystyrene Particles at Various Salinities, *Front. Mar. Sci.*, 2021, **8**, 1–14, DOI: 10.3389/fmars.2021.671802.

21 A. T. K. Tran, T. T. Pham, Q. H. Nguyen, N. T. T. Hoang, D. T. Bui, M. T. Nguyen, M. K. Nguyen and B. Van Der Bruggen, From waste disposal to valuable material: sulfonating polystyrene waste for heavy metal removal, *J. Environ. Chem. Eng.*, 2020, **8**, 104302, DOI: 10.1016/j.jece.2020.104302.

22 I. K. Ogemdi and I. K. Ogemdi, Removal of Heavy Metals from Their Solution Using Polystyrene Adsorbent (Foil Take-Away Disposable Plates), *Int. J. Environ. Chem.*, 2018, **2**, 29–38, DOI: 10.11648/j.ijec.20180202.11.

23 A. Marey, M. Adel, A. M. A. El Naggar, A. A. El-Zahhar and M. H. Taha, Nickel-hydroxide-encapsulated polyacrylamide as a novel adsorptive composite for the capture of methylene blue from wastewater, *Dalton Trans.*, 2023, **52**, 14194–14209, DOI: 10.1039/D3DT02696E.

24 A. S. A. Bakr, H. I. Al-Shafey, E. I. Arafa and A. M. A. El Naggar, Synthesis and Characterization of Polymerized Acrylamide Coupled with Acrylamido-2-Methyl-1-Propane Sulfonic Acid-Montmorillonite Structure as a Novel Nanocomposite for Cd (II) Removal from Aqueous Solutions, *J. Chem. Eng. Data*, 2020, **65**, 4079–4091, DOI: 10.1021/acs.jced.0c00385.

25 A. Marey, W. S. Gado, A. G. Soliman, A. M. Masoud, A. A. El-Zahhar, G. A. A. M. Al-Hazmi, M. H. Taha and A. M. A. El Naggar, Efficient removal of methylene blue dye from wastewater specimen using polystyrene coated nanoparticles of silica, *Inorg. Chem. Commun.*, 2024, **160**, 112018, DOI: 10.1016/J.INOCHE.2024.112018.

26 M. Adel, A. M. A. El Naggar, A. Bakry, M. H. Hilal, A. A. El-Zahhar, M. H. Taha and A. Marey, Decoration of polystyrene with nanoparticles of cobalt hydroxide as new composites for the removal of Fe(iii) and methylene blue from industrial wastewater, *RSC Adv.*, 2023, **13**, 25334–25349, DOI: 10.1039/D3RA03794K.

27 X. Wang, K. Dai, L. Chen, J. Huang and Y. N. Liu, An ethylenediamine-modified hypercrosslinked polystyrene resin: synthesis, adsorption and separation properties, *Chem. Eng. J.*, 2014, **242**, 19–26, DOI: 10.1016/J.CEJ.2013.12.037.

28 M. Davarpanah, A. Ahmadpour, T. Rohani-Bastami and H. Dabir, Synthesis and application of diethanolamine-functionalized polystyrene as a new sorbent for the removal of *p*-toluenesulfonic acid from aqueous solution, *J. Ind. Eng. Chem.*, 2015, **30**, 281–288, DOI: 10.1016/J.JIEC.2015.05.034.

29 A. A. Elzoghby, A. Bakry, A. M. Masoud, W. S. Mohamed, M. H. Taha and T. F. Hassanein, Synthesis of polyamide-based nanocomposites using green-synthesized chromium and copper oxides nanoparticles for the sorption of uranium from aqueous solution, *J. Environ. Chem. Eng.*, 2021, **9**, 106755, DOI: 10.1016/J.JECE.2021.106755.

30 S. Ghotekar, S. Pansambal, M. Bilal, S. S. Pingale and R. Oza, Environmentally friendly synthesis of Cr_2O_3 nanoparticles: Characterization, applications and future perspective − a review, *Case Stud. Chem. Environ. Eng.*, 2021, **3**, 100089, DOI: 10.1016/J.CSCEE.2021.100089.

31 M. M. El-Maadawy, A. A. Elzoghby, A. M. Masoud, Z. M. El-Deeb, A. M. A. El Naggar and M. H. Taha, Conversion of carbon black recovered from waste tires into activated carbon *via* chemical/microwave methods for efficient removal of heavy metal ions from wastewater, *RSC Adv.*, 2024, **14**, 6324–6338, DOI: 10.1039/D4RA00172A.

32 A. F. Abou-Hadid, U. A. El-Behairy, M. M. Elmalih, E. Amdeha, A. M. A. El Naggar, M. H. Taha and A. E. M. Hussein, Production of efficient carbon fiber from different solid waste residuals for adsorption of hazardous metals from wastewater samples, *Biomass Convers. Biorefin.*, 2024, **14**, 10501–10516, DOI: 10.1007/S13399-022-03097-6/FIGURES/16.

33 E. Mahmoudi, S. Azizkhani, A. W. Mohammad, L. Y. Ng, A. Benamor, W. L. Ang and M. Ba-Abbad, Simultaneous removal of Congo red and cadmium(II) from aqueous solutions using graphene oxide–silica composite as a multifunctional adsorbent, *J. Environ. Sci.*, 2020, **98**, 151–160, DOI: 10.1016/J.JES.2020.05.013.

34 R. Bassam, A. El Hallaoui, M. El Alouani, M. Jabrane, E. H. El Khattabi, M. Tridane and S. Belaaouad, Studies on the Removal of Cadmium Toxic Metal Ions by Natural Clays from Aqueous Solution by Adsorption Process, *J. Chem.*, 2021, **2021**, 7873488, DOI: 10.1155/2021/7873488.

35 D. Kumar, J. Pandey and A. Kumar, Enhanced photocatalytic removal of Cd(II) from aqueous solution using Bi/S co-doped carbon quantum dots, *Mater. Sci. Energy Technol.*, 2024, **7**, 9–18, DOI: 10.1016/J.MSET.2023.06.004.

36 I. Ahmad, M. J. Akhtar, I. B. K. Jadoon, M. Imran, M. Imran and S. Ali, Equilibrium modeling of cadmium biosorption from aqueous solution by compost, *Environ. Sci. Pollut. Res.*, 2017, **24**, 5277–5284, DOI: 10.1007/S11356-016-8280-Y/METRICS.

37 A. F. Abou-Hadid, U. A. El-Behairy, M. M. Elmalih, E. Amdeha, A. M. A. E. Naggar, M. H. Taha and A. E. M. Hussein, Conversion of corn shell as biomass solid waste into carbon species for efficient decontamination of wastewater *via* heavy metals adsorption, *Biomass Convers. Biorefin.*, 2024, **14**, 16435–16449, DOI: 10.1007/S13399-023-04057-4/FIGURES/12.

38 M. H. Taha, A. M. Masoud, Y. M. Khawassek, A. E. M. Hussein, H. F. Aly and E. Guibal, Cadmium and iron removal from phosphoric acid using commercial resins for purification purpose, *Environ. Sci. Pollut. Res.*, 2020, **27**, 31278–31288, DOI: 10.1007/S11356-020-09342-7/TABLES/4.

39 C. Yao and T. Chen, A film-diffusion-based adsorption kinetic equation and its application, *Chem. Eng. Res. Des.*, 2017, **119**, 87–92, DOI: 10.1016/J.CHERD.2017.01.004.

40 Q. Hu, S. Pang and D. Wang, In-depth Insights into Mathematical Characteristics, Selection Criteria and Common Mistakes of Adsorption Kinetic Models: A Critical

Review, *Sep. Purif. Rev.*, 2022, **51**, 281–299, DOI: **10.1080/15422119.2021.1922444**.

41 J. N. Wekoye, W. C. Wanyonyi, P. T. Wangila and M. K. Tonui, Kinetic and equilibrium studies of Congo red dye adsorption on cabbage waste powder, *Environ. Chem. Ecotoxicol.*, 2020, **2**, 24–31, DOI: **10.1016/J.ENCECO.2020.01.004**.

42 J. Wang and X. Guo, Adsorption isotherm models: Classification, physical meaning, application and solving method, *Chemosphere*, 2020, **258**, 127279, DOI: **10.1016/J.CHEMOSPHERE.2020.127279**.

43 M. A. Al-Ghouti and D. A. Da'ana, Guidelines for the use and interpretation of adsorption isotherm models: a review, *J. Hazard. Mater.*, 2020, **393**, 122383, DOI: **10.1016/J.JHAZMAT.2020.122383**.

44 Y. Wang, C. Wang, X. Huang, Q. Zhang, T. Wang and X. Guo, Guideline for modeling solid-liquid adsorption: Kinetics, isotherm, fixed bed, and thermodynamics, *Chemosphere*, 2024, **349**, 140736, DOI: **10.1016/J.CHEMOSPHERE.2023.140736**.

45 S. G. Chung, J. C. Ryu, M. K. Song, B. An, S. B. Kim, S. H. Lee and J. W. Choi, Modified composites based on mesostructured iron oxyhydroxide and synthetic minerals: a potential material for the treatment of various toxic heavy metals and its toxicity, *J. Hazard. Mater.*, 2014, **267**, 161–168, DOI: **10.1016/J.JHAZMAT.2013.12.056**.

46 S. Chatterjee, I. Sivareddy and S. De, Adsorptive removal of potentially toxic metals (cadmium, copper, nickel and zinc) by chemically treated laterite: single and multicomponent batch and column study, *J. Environ. Chem. Eng.*, 2017, **5**, 3273–3289, DOI: **10.1016/J.JECE.2017.06.029**.

47 S. Jawad Alhamd, M. Nsaif Abbas, M. Manteghian, T. Atta Ibrahim, K. Dawood Salman Jarmondi, S. J. Alhamd, M. N. Abbas, T. A. Ibrahim and K. D. Jarmondi, Treatment of Oil Refinery Wastewater Polluted by Heavy Metal Ions *via* Adsorption Technique using Non-Valuable Media: Cadmium Ions and Buckthorn Leaves as a Study Case, *Karbala Int. J. Mod. Sci.*, 2024, **10**(1), 1–18, DOI: **10.33640/2405-609X.3334**.

48 R. Kundu, C. Biswas, J. Ahmed, J. Naime and H. Ara, A Study on the Adsorption of Cadmium(II) from Aqueous Solution onto Activated Carbon Originated from Bombax ceiba Fruit Shell, *J. Chem. Health Risks*, 2020, **10**, 243–252, DOI: **10.22034/jchr.2020.1903764.1154**.

49 H. Abbasi, F. Salimi and F. Golmohammadi, Removal of Cadmium from Aqueous Solution by Nano Composites of Bentonite/TiO2 and Bentonite/ZnO Using Photocatalysis Adsorption Process, *Silicon*, 2020, **12**, 2721–2731, DOI: **10.1007/S12633-019-00372-6/METRICS**.

50 A. Almasi, M. Omidi, M. Khodadadian, R. Khamutian and M. B. Gholivand, Lead(II) and cadmium(II) removal from aqueous solution using processed walnut shell: kinetic and equilibrium study, *Toxicol. Environ. Chem.*, 2012, **94**, 660–671, DOI: **10.1080/02772248.2012.671328**.

51 R. Karthik and S. Meenakshi, Chemical modification of chitin with polypyrrole for the uptake of Pb(II) and Cd(II) ions, *Int. J. Biol. Macromol.*, 2015, **78**, 157–164, DOI: **10.1016/J.IJBIOMAC.2015.03.041**.

52 Z. H. Khan, M. Gao, W. Qiu and Z. Song, Properties and adsorption mechanism of magnetic biochar modified with molybdenum disulfide for cadmium in aqueous solution, *Chemosphere*, 2020, **255**, 126995, DOI: **10.1016/J.CHEMOSPHERE.2020.126995**.

53 A. N. Ebelegi, N. Ayawei, D. Wankasi, A. N. Ebelegi, N. Ayawei and D. Wankasi, Interpretation of Adsorption Thermodynamics and Kinetics, *Open J. Phys. Chem.*, 2020, **10**, 166–182, DOI: **10.4236/OJPC.2020.103010**.

54 X. Cui, S. Fang, Y. Yao, T. Li, Q. Ni, X. Yang and Z. He, Potential mechanisms of cadmium removal from aqueous solution by Canna indica derived biochar, *Sci. Total Environ.*, 2016, **562**, 517–525, DOI: **10.1016/J.SCITOTENV.2016.03.248**.

55 Y. Deng, S. Huang, C. Dong, Z. Meng and X. Wang, Competitive adsorption behaviour and mechanisms of cadmium, nickel and ammonium from aqueous solution by fresh and ageing rice straw biochars, *Bioresour. Technol.*, 2020, **303**, 122853, DOI: **10.1016/J.BIORTECH.2020.122853**.

56 B. T. Iber, V. T. Okomoda, S. A. Rozaimah and N. A. Kasan, Eco-friendly approaches to aquaculture wastewater treatment: assessment of natural coagulants vis-a-vis chitosan, *Bioresour. Technol. Rep.*, 2021, **15**, 100702, DOI: **10.1016/J.BITEB.2021.100702**.

57 X. Xu, X. Cao and L. Zhao, Comparison of rice husk- and dairy manure-derived biochars for simultaneously removing heavy metals from aqueous solutions: role of mineral components in biochars, *Chemosphere*, 2013, **92**, 955–961, DOI: **10.1016/J.CHEMOSPHERE.2013.03.009**.